An efficient method to establish electrostatic screening lengths of Restricted Primitive Model electrolytes

Electronic Supplementary Material (ESI)

Jan Forsman*, David Ribar*, and Clifford E. Woodward**

*Computational Chemistry, Lund University
P.O.Box 124, S-221 00 Lund, Sweden
**School of Physical, Environmental and Mathematical Sciences
University College, University of New South Wales, ADFA
Canberra ACT 2600, Australia

February 6, 2024

1 Renormalized OZ-HNC

1.1 Brief introduction

For a two component ionic system, denoted by indexes + and − respectively, the Ornstein-Zernike (OZ) equation takes the following matrix form in k-space,[1] with a hat symbol indicating the respective Fourier transformed functions

$$\hat{\mathbf{H}}(k) = \hat{\mathbf{C}}(k) + \hat{\mathbf{C}}(k)\boldsymbol{\rho}\hat{\mathbf{H}}(k) \tag{1}$$

where $\hat{\mathbf{H}}$ and $\hat{\mathbf{C}}$ denote 2×2 matrices of total and direct correlation functions, defined as

$$\hat{\mathbf{H}}(k) = \begin{bmatrix} \hat{h}_{++}(k) & \hat{h}_{-+}(k) \\ \hat{h}_{+-}(k) & \hat{h}_{--}(k) \end{bmatrix} \tag{2}$$

$$\hat{\mathbf{C}}(k) = \begin{bmatrix} \hat{c}_{++}(k) & \hat{c}_{-+}(k) \\ \hat{c}_{+-}(k) & \hat{c}_{--}(k) \end{bmatrix} \tag{3}$$

and $\boldsymbol{\rho}$ describes the number densities via

$$\boldsymbol{\rho} = \begin{bmatrix} \rho_+ & 0 \\ 0 & \rho_- \end{bmatrix} \tag{4}$$

Due to a symmetric system, the non-diagonal correlation functions are identical, with $\hat{h}_{+-}(k) = \hat{h}_{-+}(k)$ and $\hat{c}_{+-}(k) = \hat{c}_{-+}(k)$. To ensure electroneutrality, the number densities are equal $\rho_+ = \rho_-$. The renormalisation of the OZ equation is preceded by splitting the the long ranged Coulomb pair potential into a short and long ranged potential (with i, j denoting + or -)

$$u_{ij}(r) = u_{ij}^{(s)}(r) + u_{ij}^{(l)}(r) \tag{5}$$

where the short-ranged potential $u_{ij}^{(s)}$ is defined as a hard sphere potential of the classical form

$$u_{ij}^{(s)}(r) = u_{ij}^{HS}(r) = \begin{cases} \infty; & r < \sigma_{ij} \\ 0; & r > \sigma_{ij} \end{cases} \tag{6}$$

and $u_{ij}^{(l)}$ denotes the long range potential, whose matrix form is denoted with the matrix $\boldsymbol{\psi}(r)$. We now move onto defining Fourier transformed matrix elements of the renormalized OZ equation. By using the Fourier transformed long range potential $\hat{\boldsymbol{\psi}}(k)$, we define a short ranged total correlation matrix

$$\hat{\mathbf{C}}^{(s)}(k) = \hat{\mathbf{C}}(k) - \hat{\boldsymbol{\psi}}(k) \tag{7}$$

and the hypervertex function $\hat{\mathbf{V}}$ via

$$\hat{\mathbf{V}}^{-1}(k) = \boldsymbol{\rho}^{-1} - \hat{\boldsymbol{\psi}}(k) \tag{8}$$

used in the construction of the $\hat{\mathbf{Q}}$ and $\hat{\mathbf{H}}^{(s)}$ functions by

$$\boldsymbol{\rho}\hat{\mathbf{Q}}(k)\boldsymbol{\rho} = \hat{\mathbf{V}}(k) - \boldsymbol{\rho} \tag{9}$$

$$\hat{\mathbf{H}}^{(s)}(k) = \hat{\mathbf{H}}(k) - \hat{\mathbf{Q}}(k) \tag{10}$$

For numerical simplicity, we define a new $\hat{\boldsymbol{\tau}}$ function as

$$\hat{\boldsymbol{\tau}}(k) = \hat{\mathbf{H}}^{(s)}(k) - \hat{\mathbf{C}}^{(s)}(k) \tag{11}$$

leading to the final renormalised form of the OZ equation, used in direct numerical iteration, eq. 12.

$$\boxed{\boldsymbol{\rho}\hat{\boldsymbol{\tau}}(k)\boldsymbol{\rho} = \hat{\mathbf{V}}(k)\hat{\mathbf{C}}^{(s)}(k)\left[\mathbf{I} - \hat{\mathbf{V}}(k)\hat{\mathbf{C}}^{(s)}(k)\right]^{-1}\hat{\mathbf{V}}(k) - \boldsymbol{\rho}\hat{\mathbf{C}}^{(s)}(k)\boldsymbol{\rho}} \tag{12}$$

The exact renormalised closure relation for the system, written in r-space, is defined via Eq.(14).

$$c_{ij}^{(s)}(r) = \exp\left[-\beta u_{ij}^{(s)}(r) + \tau_{ij}(r) + q_{ij}(r) + \mathcal{B}_{ij}(r)\right] - 1 - \tau_{ij}(r) - q_{ij}(r) \tag{13}$$

For the HNC closure, the bridge graphs are set to equal zero, $\mathcal{B}(r) = 0$, simplifying the closure to the following form used in the numerical procedure, Eq.(14).

$$\boxed{c_{ij}^{(s)}(r) = \exp\left[-\beta u_{ij}^{(s)}(r) + \tau_{ij}(r) + q_{ij}(r)\right] - 1 - \tau_{ij}(r) - q_{ij}(r)} \tag{14}$$

We define ψ_{ij} as a Coulomb potential

$$\psi_{ij}(r) = -\frac{z_i z_j l_B}{r} \tag{15}$$

and the corresponding q_{ij} potential as a screened Coulomb potential via

$$q_{ij}(r) = -z_i z_j l_B \frac{\exp\left(-\kappa_D^{-1} r\right)}{r} \tag{16}$$

with z_i, z_j denoting the nominal charge (1 or -1 used in this work), $l_B = \frac{e_0^2}{4\pi\varepsilon_0\varepsilon_r k_B T}$ the Bjerrum length, and κ_D the Debye screening length, obtained via

$$\kappa_D = \sqrt{4\pi l_B(\rho_+ z_+^2 + \rho_- z_-^2)} \tag{17}$$

The analytical form of the Fourier transformed screened Coulomb potential is used

$$\hat{q}_{ij}(k) = -\frac{4\pi z_i z_j l_B}{k^2 + \kappa_D^2} \tag{18}$$

1.2 Numerical implementation

For the numerical solution of the coupled matrix equations, Eqs. (12) and (14), a direct iteration method via Picard mixing was used. Real space discretization was achieved with 2^{18} points at a 0.005 Å spacing interval, in order to comply with the requirement of zeroth and second moments equalling zero (ensuring electroneutrality). [2–5]

The initial $\tau_{ij}(r)$ functions were initialised with 0 arrays, and the potential functions according to the definitions. Via Eq.(14), the initial short range direct correlation functions $c_{ij}^{(s)}(r)$ were computed. Both $\tau_{ij}(r)$ and $c_{ij}^{(s)}(r)$ functions are Fourier transformed into corresponding $\hat{\tau}_{ij}(k)$ and $\hat{c}_{ij}^{(s)}(k)$ functions. The renormalised OZ equation, Eq.(12), is used to compute new $\hat{\tau}_{ij}(k)$ functions, which are then Fourier transformed back into r-space and mixed with the previous iteration via the Picard mixing procedure. The mixed result is used to compute new $c_{ij}^{(s)}(r)$ functions via Eq.(14).

We define a cost function $\mathcal{L}$ used for the convergence criteria as

$$\mathcal{L} = \delta r \sqrt{\sum_{i,j}\left(\tau'_{ij}(r) - \tau_{ij}(r)\right)^2} \tag{19}$$

with δr defining the real space discretization spacing interval and the prime denoting the new iteration. We impose a convergence criteria of $\mathcal{L} < 10^{-6}$.

Once convergence is achieved, we obtain the radial distribution functions with following relations

$$\mathbf{H}(r) = \boldsymbol{\tau}(r) + \mathbf{C}^{(s)}(r) + \mathbf{Q}(r) \tag{20}$$

$$g_{ij}(r) = h_{ij}(r) + 1 \tag{21}$$

and for calculating the direct correlation function, we use

$$\mathbf{C}(r) = \mathbf{C}^{(s)}(r) + \boldsymbol{\psi}(r) \tag{22}$$

1.3 Results

1.3.1 Comparison of MC and OZ-HNC

As can be seen from Figures 1 and 2, OZ-HNC quantitatively describes the radial distribution functions obtained from MC results.

1.3.2 Extracting the screening lengths

We extracted the screening lengths with a linear fit on the $\ln[r\Delta g(r)]$ vs. r plots. Figure 3 presents the procedure of extracting the κ values. The screening length was difficult to extract for higher concentrations ($c > 1$ M) due to extensive curvature in the $\ln[r\Delta g(r)]$ data, thereby presenting a challenge to select the linear interval appropriate for fitting a linear model. The underestimation of the screening lengths obtained via OZ-HNC in comparison to the Widom method (presented in the main article) should therefore be explained as a statistical error of fitting.

2 Statistical properties of standard and inverse Widom

Here, we briefly illustrate that the inverse Widom is computationally much more efficient than its standard (insertion) counterpart, at least for systems with strong electrostatic coupling. In Figure 4, we compare results from the two methods, for our low-dielectric system ($\epsilon_r = 11.04$) and a concentration of 100mM. The displacement (which actually helps for illustrative purposes) between the two sets of curves stem from the irrelevant (for our purposes) excluded volume contribution. The inverse Widom method is clearly superior.

On the other hand, in systems with weak electrostatic coupling, the methods are essentially equivalent, which is demonstrated in Figure 5, where we have removed the excluded volume contribution to the insertion chemical potential, i.e. the curves are not shifted. The agreement suggests that either method works equally well at "aqueous" conditions.

3 Comparing the decay of $\Delta g(r)$ and $|\Delta g(r)|$

In the scientific literature, one commonly finds long-range analyses of $|\Delta g(r)|$, rather than $\Delta g(r)$. An advantage with the former is that it permits logarithmic fits, which of course is relevant for an assumed Yukawa tail. However, we would argue that it is better to perform runnning averages of noisy data, and simply limit any fit to a region in which $\Delta g(r)$ is positive. This is illustrated in Figure 6. Note how the running averages for $\Delta g(r)$ and $|\Delta g(r)|$ start to deviate at about 50 Å, which thus (roughly) marks the upper limit for appropriate analyses of $|\Delta g(r)|$. On the other hand, the running average of $\Delta g(r)$ stays positive up to about twice this separation.

References

[1] T. Ichiye and A. D. J. Haymet, *The Journal of Chemical Physics*, 1988, **89**, 4315–4324.

[2] J. Rasaiah, *Chemical Physics Letters*, 1970, **7**, 260–264.

[3] J. Stillinger, Frank H. and R. Lovett, *The Journal of Chemical Physics*, 2003, **48**, 3858–3868.

[4] A. McBride, M. Kohonen and P. Attard, *The Journal of Chemical Physics*, 1998, **109**, 2423–2428.

[5] P. Attard, *Phys. Rev. E*, 1993, **48**, 3604–3621.

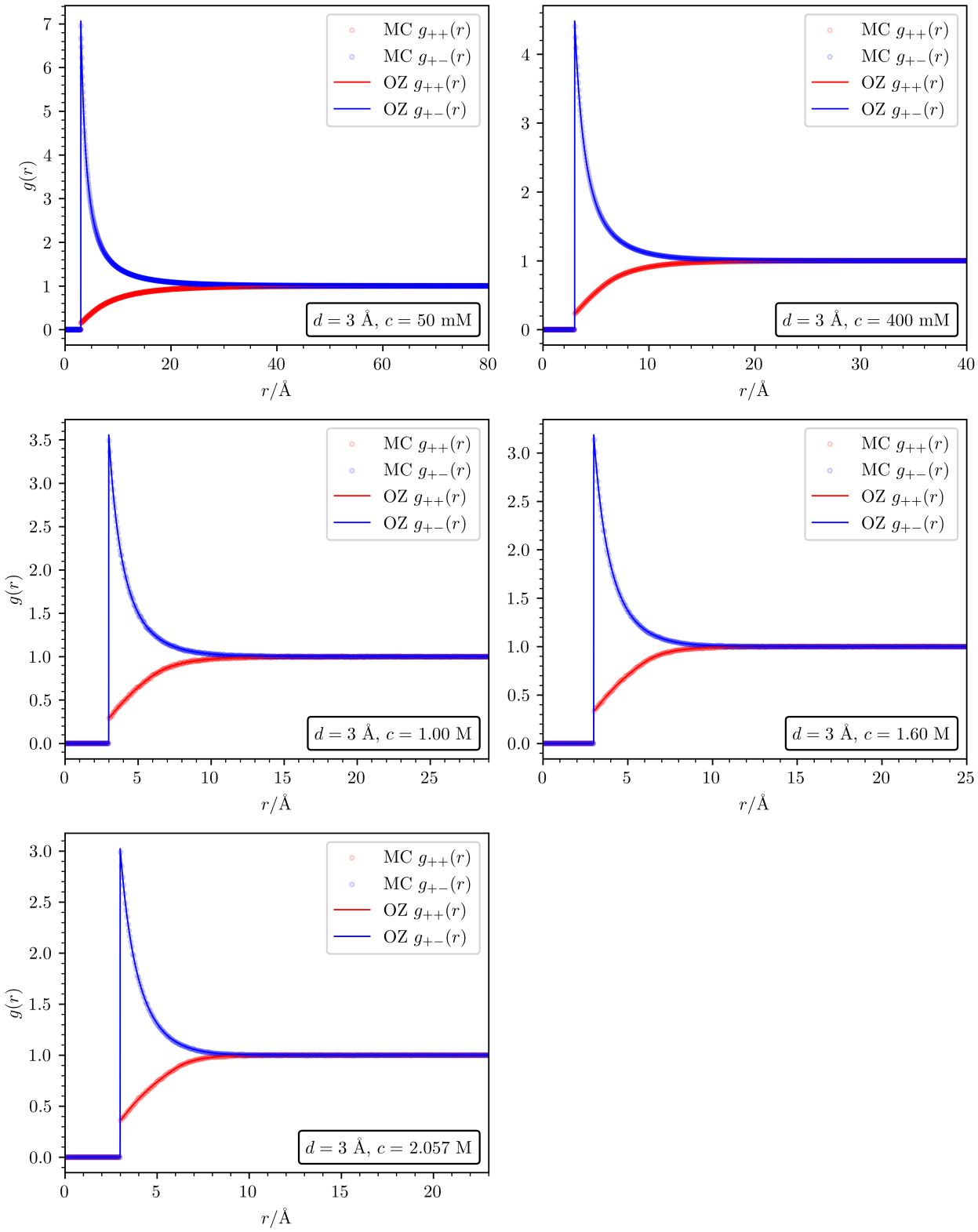

Figure 1: Comparison of MC (empty circles) and OZ-HNC results (full lines) for the 3 Å system at five concentrations.

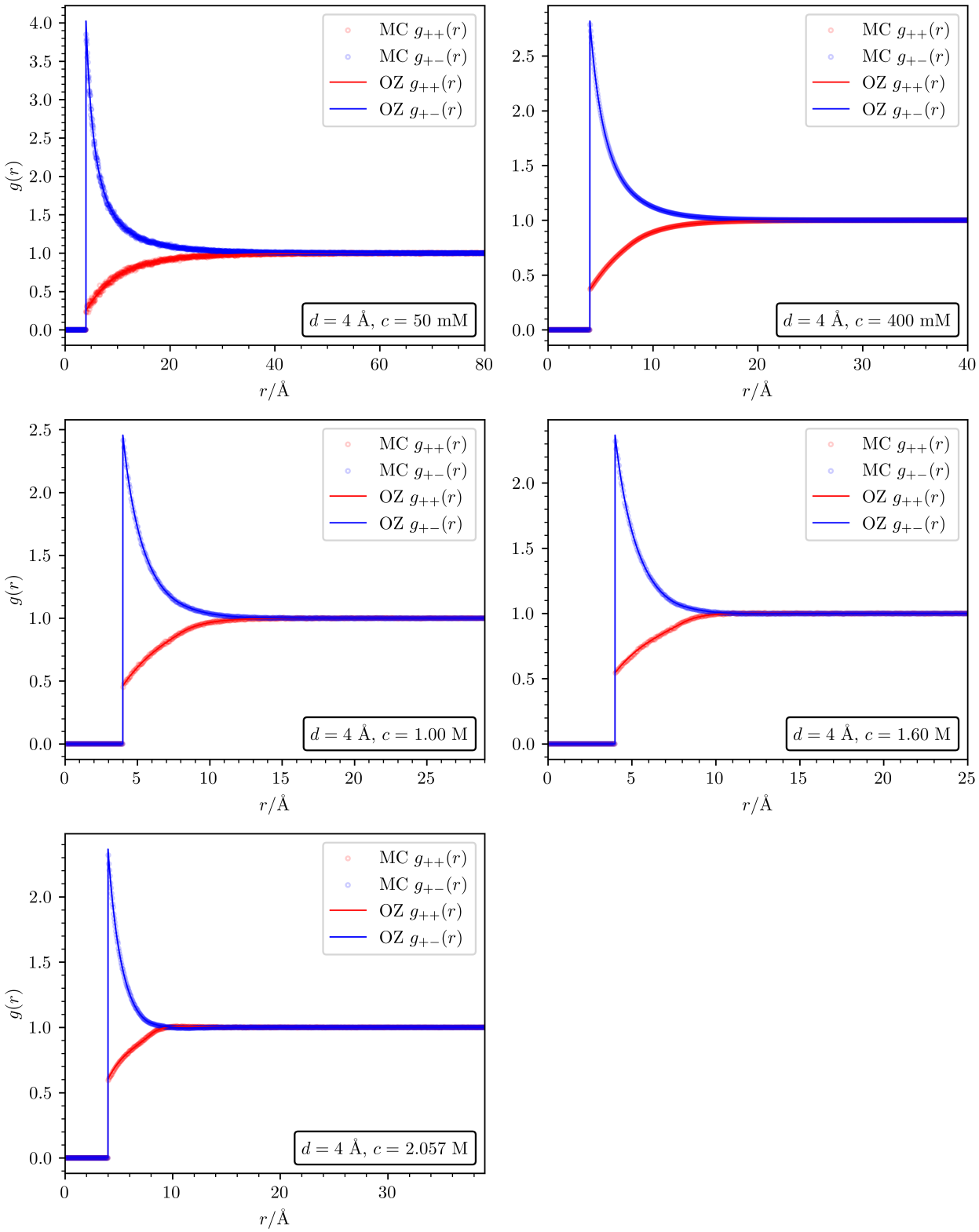

Figure 2: Comparison of MC (empty circles) and OZ-HNC results (full lines) for the 4 Å system at five concentrations.

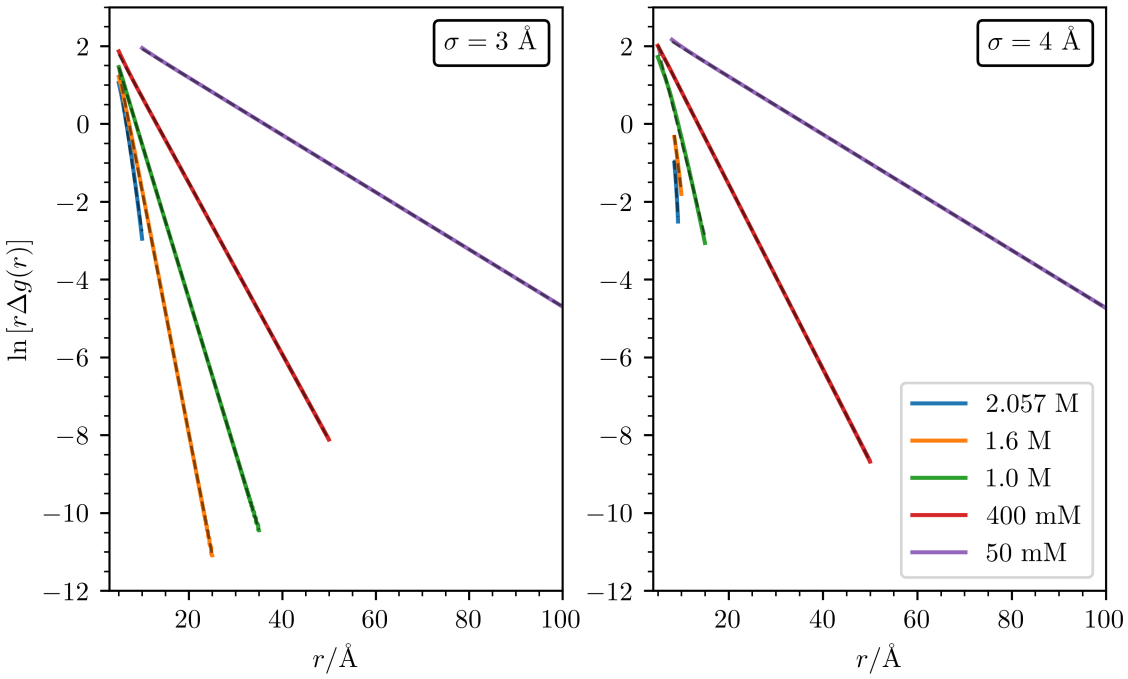

Figure 3: Linear fits for extracting the screening length from the OZ-HNC results, with the linear fit depicted by the dashed line.

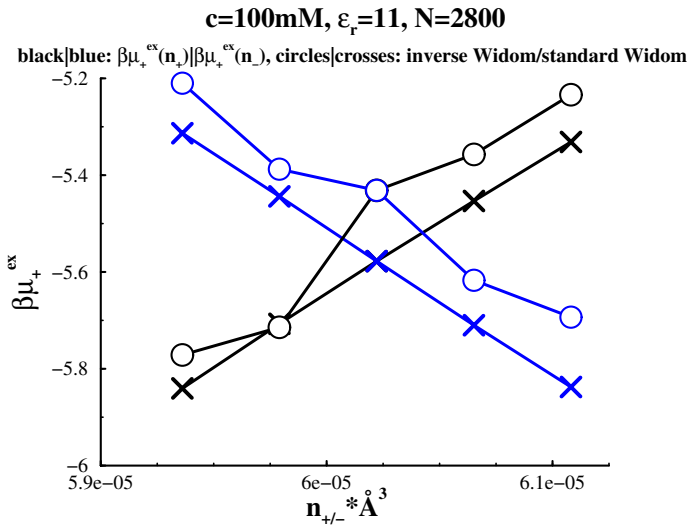

Figure 4: Comparing results from standard and inverse Widom, in a low-dielectric implicit solvent. Note that the results are shifted, since the inverse method neglects excluded volume contributions. This shift is irrelevant as we aim for the electrostatic screening length, which only requires the difference between slopes.

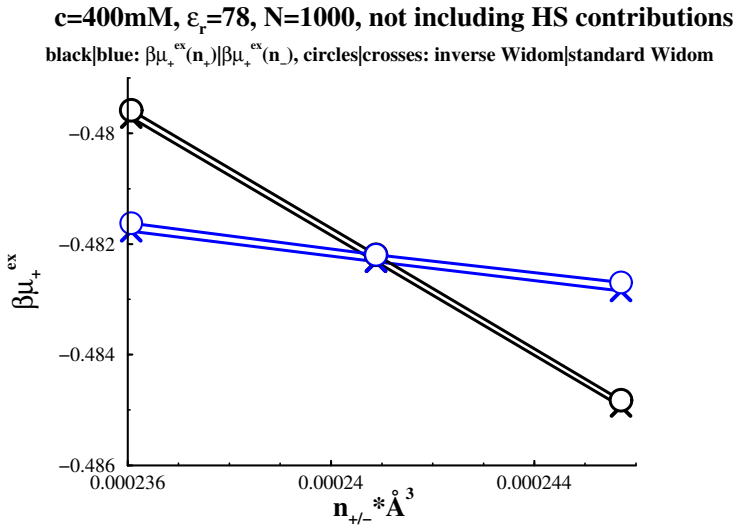

Figure 5: Comparing results from standard and inverse Widom, at "aqueous" conditions. The hard-sphere contribution has been subtracted from the standard Widom data.

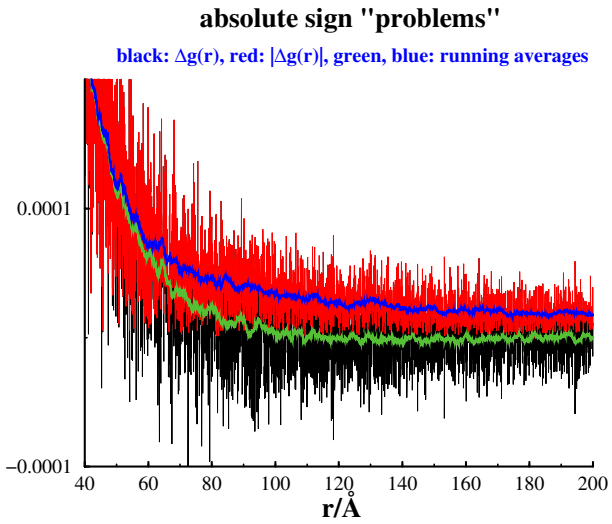

Figure 6: Comparing results for the long-ranged part of $\Delta g(r)$ and $|\Delta g(r)|$. Thick curves are running averages.